THE JOURNAL OF PHYSICAL CHEMISTRY C

Article

pubs.acs.org/JPCC

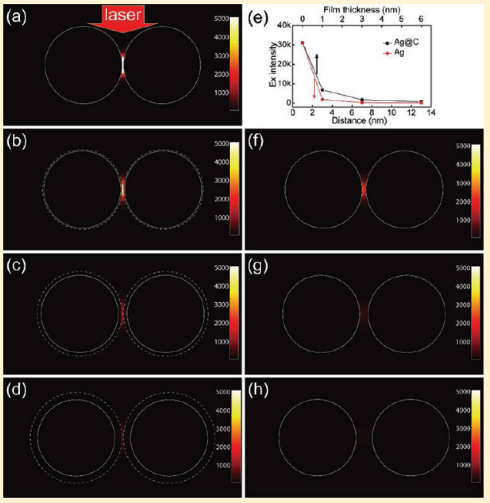
Ag@C Core–Shell Colloidal Nanoparticles Prepared by the Hydrothermal Route and the Low Temperature Heating–Stirring Method and Their Application in Surface Enhanced Raman Scattering

Dawei Li, Shifa Wu, Qiao Wang, Yongkuan Wu, Wei Peng, and Lujun Pan*

School of Physics and Optoelectronic Technology, Dalian University of Technology, Dalian, Liaoning, 116024, PR China

Supporting Information

ABSTRACT: Silver nanoparticles (AgNPs) with diameters in the range 40–80 nm have been synthesized by the hydrothermal route and the low temperature heating–stirring method. The influences of reaction time, reactant concentration, and temperature on the AgNP growth have been systemically studied. Experimental surface enhanced Raman scattering (SERS) results show that AgNPs prepared under different temperature and time exhibit a large difference in enhanced SERS signals for rhodamine 6G (10^{-6} M). Ag@C core–shell NPs have been proved to be formed by using the above two methods, and the carbon shell thickness is gradually increased with increasing reaction time and temperature. It is found that Ag@C NPs with a thick shell (more than 3 nm) have a very low SERS activity, while those with an ultrathin film (less than 1 nm) have a high SERS activity, indicating that carbon shell thickness is a key factor affecting the SERS, which has also been evaluated by finite-difference time-domain simulation. The existence of an ultrathin carbon shell around the AgNP can decrease its surface electric property; then Ag@C NP aggregates are easily formed which may produce the higher hot spots than the bare AgNPs. In addition, this kind of Ag@C NPs exhibits a long SERS-active shelf life (6 months), because the carbon shell can protect AgNPs from oxidation.



1. INTRODUCTION

It is known that metal nanoparticles (NPs) have unique optical,[1] magnetic,[2] and catalytic properties,[3] which are substantially different from the bulk materials. Due to these excellent properties, metal NPs are expected to be used in data storage, electromagnetic wave absorbers, and catalysts, etc. It should be noted that noble metal NPs (such as gold and silver) also exhibit another phenomenon known as surface enhanced Raman scattering (SERS) which was first discovered by Jeanmarie et al. in 1977.[4] SERS is considered to be a direct and sensitive technique and has been actively explored in the past few years.[5,6] Compared with gold, silver is the most efficient metal for SERS application.[7] So far, silver NPs (AgNPs) have often been synthesized by aqueous phase reduction of silver nitrate in the presence of stabilizers or protectants, such as polyvinylpyrrolidone (PVP),[8,9] polyvinyl alcohol,[10] cetyl trimethyl ammonium bromide (CTAB),[11] etc. During the reduction reactions, sodium borohydride, sodium citrate, ascorbic acid, methanal, and alcohol were usually used as the reducing agents. It is also known that glucose has some reduction activities, because it contains an aldehyde or potential aldehyde group. It is considered that glucose has the advantages of being environmentally friendly and a mild reducing agent, which enables the reaction kinetics to be easily controlled. To our knowledge, there have been some reports about the synthesis of Ag nanostructures by using glucose as the reducing agents. For example, Wang et al. have prepared silver nanowire by reducing silver chloride with glucose in the absence of any surfactant or polymers.[12] Similarly, Liu and Mori et al. have successfully prepared uniform spherical AgNPs by reducing silver nitrate or silver-contained glass powder with glucose by the hydrothermal route, where Liu et al. briefly discussed the effects of protectant and reaction temperature on the morphologies of the grown AgNPs.[13,14] However, they did not discuss in detail the influences of other reaction conditions, such as solution concentration and reaction time, on the AgNP growth. More importantly, the SERS activity of these AgNPs has not been known yet.

Recently, core–shell nanoparticles have been of great interest in many studies.[15] Li et al. have prepared gold NPs with an ultrathin silica or alumina shell and investigated their SERS activity.[16] Wang et al. have prepared ultrathin diamond-like

Received: February 23, 2012
Revised: May 2, 2012
Published: May 3, 2012

 © 2012 American Chemical Society

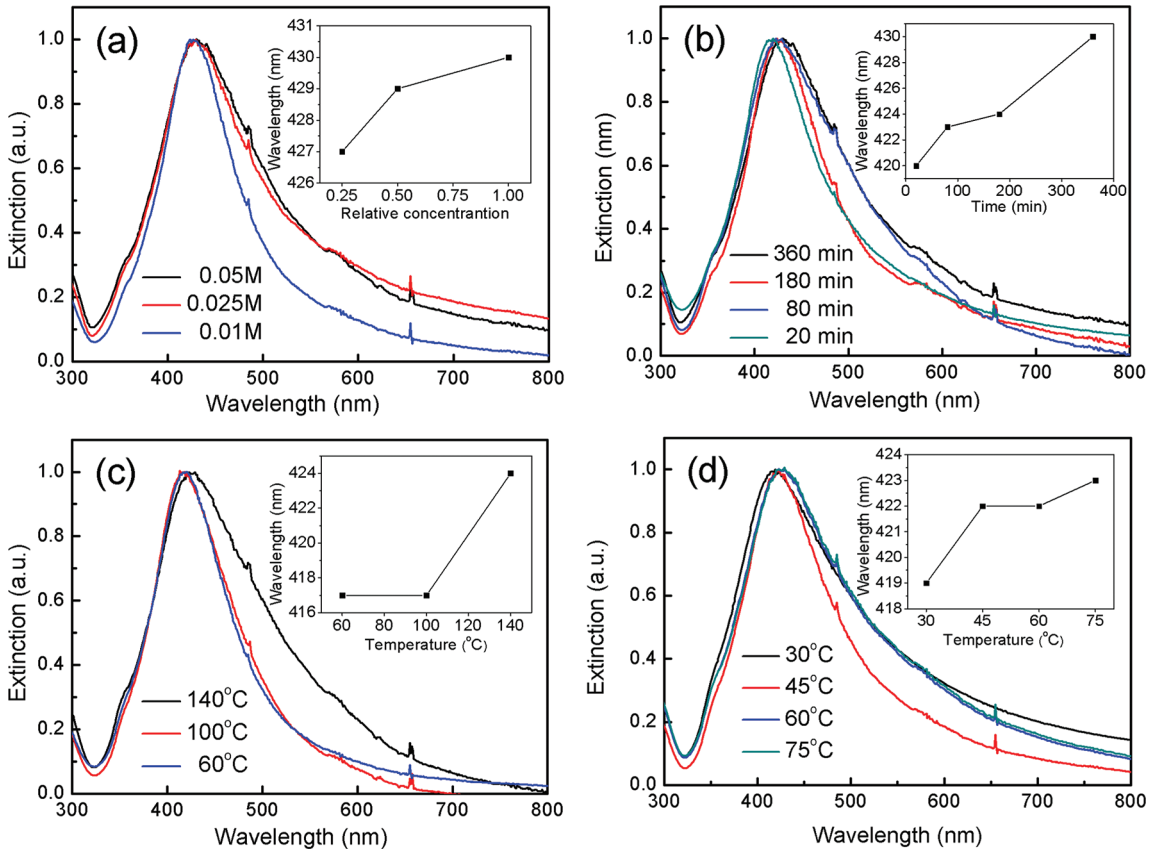


Figure 1. UV−visible absorption spectra of as-prepared AgNPs under different reaction parameters: (a) AgNP(HT,140,360) prepared with different $AgNO_3$ solution concentrations; (b) AgNPs prepared by the HT method at 140 °C for different heating times; (c) AgNPs prepared by the HT method under different reaction temperatures for 80 min; (d) AgNPs prepared by the HS method under different reaction temperatures for 60 min.

carbon film coated metal NP-based SERS substrates using a combined nanosphere lithography and filtered cathodic vacuum arc method.[17,18]

In this paper, we have described a facile and versatile strategy for the growth of AgNPs under hydrothermal and low temperature heating−stirring conditions using glucose as the reducing agent and PVP as the stabilizer, and discussed the influences of reaction conditions (time, temperature, reactant concentration) on the AgNP growth. It is found that reaction time and temperature can influence the NP sizes greatly. AgNPs with an ultrathin carbon shell have been proved to be formed by using the above two methods. SERS experimental results show that AgNPs prepared under different temperatures and times exhibit a large difference in SERS signals. Carbon shells with different thickness formed on the AgNP surfaces are found to be the main cause in the SERS difference, which has also been evaluated by the finite-difference time-domain (FDTD) simulation.

2. EXPERIMENTAL SECTION

2.1. AgNP Synthesis. *Hydrothermal (HT) Method.* A 0.5 g portion of PVP was dissolved in 10 mL of deionized water. Then, 5 mL of aqueous NaOH (0.1 M) and 5 mL of aqueous glucose (0.2 M) were successively put into the PVP solution and stirred for 5 min. A 10 mL portion of aqueous $AgNO_3$ (0.05 M) was dropped into the above mixed solution during the stirring process, and the solution turned black because of the formation of AgO. After stirring for another 10 min, the reaction solution was transformed to a 50 mL Teflon-sealed autoclave and maintained at 60−140 °C for 20−360 min. In addition, AgNPs were also prepared by using reaction solution with $AgNO_3$/glucose solution concentrations of 0.025/0.1 M and 0.01/0.04 M, where the molar ratio of $AgNO_3$ to glucose was kept unchanged. After the reaction, the autoclave was cooled to room temperature. The suspension was centrifuged at 8000 rpm for 10 min, and the resulting precipitates (AgNPs) were washed with aqueous water. The above centrifugation and washing processes were repeated four times, and finally, the formed AgNPs were stored in water or ethanol.

Heating−Stirring (HS) Method. The preparation of reaction solution is similar to that of the HT method. The black reaction solution was stirred constantly at a temperature of 30−75 °C for 60 min. Then, the resulting precipitates were washed in accordance with the HT method.

For convenience of discussion, the as-prepared AgNPs were labeled as AgNP(M,T,D), where M, T, and D represent method, heating temperature (units: °C), and heating duration (units: min), respectively.

2.2. SERS Measurement. Rhodamine 6G (R6G) with a concentration of 10^{-6}−10^{-7} M was selected as the probe molecule. First, SERS spectra were mainly detected in solution phase. For all the AgNPs prepared under different reaction conditions, their relative concentration was made basically the same by dilution. The aqueous AgNPs were mixed with R6G solution (10^{-6} M) with different volume ratios (keeping the volume of R6G unchanged) and ultrasonically vibrated for 30 min. Then, the capillary glass tube was used for absorbing small amounts of R6G/AgNP solution for SERS measurement.

dx.doi.org/10.1021/jp3018088 | J. Phys. Chem. C 2012, 116, 12283−12294

In addition, a kind of SERS substrate was prepared as follows: 10 μL of AgNP(HS,60,60) alcoholic solution was spin-coated on a Si substrate (size: 8 × 8 mm^2) with a rotating speed of 1000−2000 rpm and dried at 50 °C for 30 min. The AgNP(HS,60,60) film substrate was immersed in the R6G solution (10^{-7} M) for a few hours and then dried at 50 °C.

2.3. Characterization. The products were analyzed by UV−visible spectrometer (HP8453, USA), atomic force microscope (AFM; Agilent PicoPlus II, Agilent, Santa Clara, CA), transmission electron microscope (TEM, JEM-2000EX), high-resolution transmission electron microscope (HRTEM; JEM-2000EX), scanning electron microscope (SEM, Nova NanoSEM 450, FEI), X-ray photoelectron spectroscopy (XPS, ESCALAB250, Thermo VG), and Raman spectrometer (Renishaw inVia plus, Renishaw, Gloucestershire, U.K.). For SEM and AFM characterization, the as-prepared AgNPs were spin-coated on the Si substrate, and we did not coat any discharging layer (typically Au−Pd or carbon) on the substrate. All the Raman testing experiments were carried out under the same conditions as follows: a 632.8 nm He−Ne laser with a power of 3.28 mW was used as exciting light, and the spectra were recorded with an accumulation time of 10 s.

3. RESULTS AND DISCUSSION

3.1. AgNP Synthesis by HT and Low-Temperature HS Methods. It is known that the shapes and sizes of AgNPs are greatly influenced by reaction conditions. In this section, we have prepared AgNPs by the HT and HS methods and systemically investigated the effects of reactant concentration, reaction time, and temperature on the AgNP growth.

Figure 1 shows the UV−visible absorption spectra of as-prepared colloidal AgNPs under different reaction parameters. The UV−visible absorption spectra of as-prepared AgNP-(HT,140,360) with different $AgNO_3$ solution concentrations are shown in Figure 1a. With the increase of $AgNO_3$ concentration, only a very slight red shift of absorption peak has been observed (inset in Figure 1a), indicating that the effect of $AgNO_3$ solution concentration on the sizes of AgNPs is negligible. In this work, the molar ratio of $AgNO_3$/glucose (reducing agent) is kept unchanged. It is considered that the sizes of AgNPs mainly depend on the $AgNO_3$/glucose molar ratio, not only on the $AgNO_3$ solution concentration. It also found that the width of the absorption peaks due to surface plasma resonance (SPR) of NPs becomes narrow with decreasing the reactant concentration, which reveals that AgNPs with more uniform sizes are produced at lower concentration. It can be seen from AFM images (Figure S1, Supporting Information) and Table 1 that the average sizes of these AgNPs are almost the same, approximately 65 nm, and the size distribution is narrowed by decreasing the reaction solution concentration.

Figure 1b shows the UV−visible absorption spectra of AgNPs prepared by the HT method at 140 °C for various heating times. It is observed that the major SPR peaks of NPs show a continuous red shift from 420 to 430 nm with increase of the heating time from 20 to 360 min (inset in Figure 1b), indicating an increase in NP size. The AgNPs obtained by reactions for 20 and 180 min show relatively narrow SPR peaks, which could also be attributed to their narrow size distribution. It is seen from the AFM images (Figure S2, Supporting Information) that the average sizes of AgNPs prepared for 20, 80, and 180 min are 45, 50, and 60 nm, respectively. The size distribution of AgNPs prepared for 20 and 180 min looks more uniform than that of 80 min, which agrees well with that of the UV−visible absorption spectra.

Table 1. The Effect of Different Parameters on AgNP Size

method	parameter		SPR peak (nm)	average NP size (nm)
HT method	$AgNO_3$ concentration (140 °C, 360 min)	0.01 M	427	65
		0.025 M	429	65
		0.05 M	430	65
	time duration (0.05 M, 140 °C)	20 min	420	45
		80 min	423	50
		180 min	424	60
		360 min	430	65
	reaction temperature (0.05 M, 180 min)	60 °C	417	50
		100 °C	417	50
		140 °C	424	60
HS method	reaction temperature (0.05 M, 60 min)	30 °C	419	40
		45 °C	422	60
		60 °C	422	70
		75 °C	423	80

Figure 1c shows the UV−visible adsorption spectra of AgNPs prepared by the HT method under different temperatures. It can be inferred from the slight red shift of SPR peaks (inset in Figure 1c) that the sizes of AgNPs are not increased too much with increase of the heating temperature. The widths of SPR peaks for NPs prepared at lower temperature (60 and 100 °C) are obviously narrower than that of AgNPs prepared at 140 °C, indicating a narrow size distribution in relatively low temperature conditions. AFM images of AgNPs prepared by the HT method at 60, 100, and 140 °C for 80 min are shown in Figure S3 in the Supporting Information. It is clearly observed that the sizes of AgNPs prepared at 60 and 100 °C are similar, approximately 50 nm in diameter, which is smaller than those of NPs prepared at 140 °C.

For the AgNPs prepared by the HS method, we only investigated the effect of reaction temperature on the AgNP growth, as shown in Figure 1d. It is found that the SPR peaks of AgNPs only have a slight red shift with increase of the heating temperature and AgNPs obtained at 45 °C have the narrowest SPR peak. From the AFM images shown in Figure S4 in the Supporting Information, it is observed that AgNPs with sizes increasing from 40 to 60, 70, and 80 nm were obtained after the reaction at temperatures of 30, 45, 60, and 75 °C, respectively. Besides, AgNPs obtained at 45 °C have the most uniform size distribution, which is in agreement with the above UV−visible observation.

Additionally, Figure 2 shows the Raman spectra of colloidal AgNPs prepared by (a) the HT method and (b) the HS method. As shown in Figure 2a, two carbon-related broad peaks in Raman spectra are exhibited; one is around 1400 cm^{-1} (D-band), and the other is around 1604 cm^{-1} (G-band), which includes the bonding information of sp^2 and sp^3 site vibrations. This reveals that carbon-containing materials exist around the AgNPs and they are amorphous in nanostructure. The G-band is originated from the bond stretching of all pairs of sp^2 atoms in both rings and chains, and the D-band is originated from the breathing modes of sp^2 atoms in rings induced by disordered-activated aromatic modes of A1 symmetry.[19,20] Recently, Zhang et al. have synthesized Ag nanocubes with controllable edge

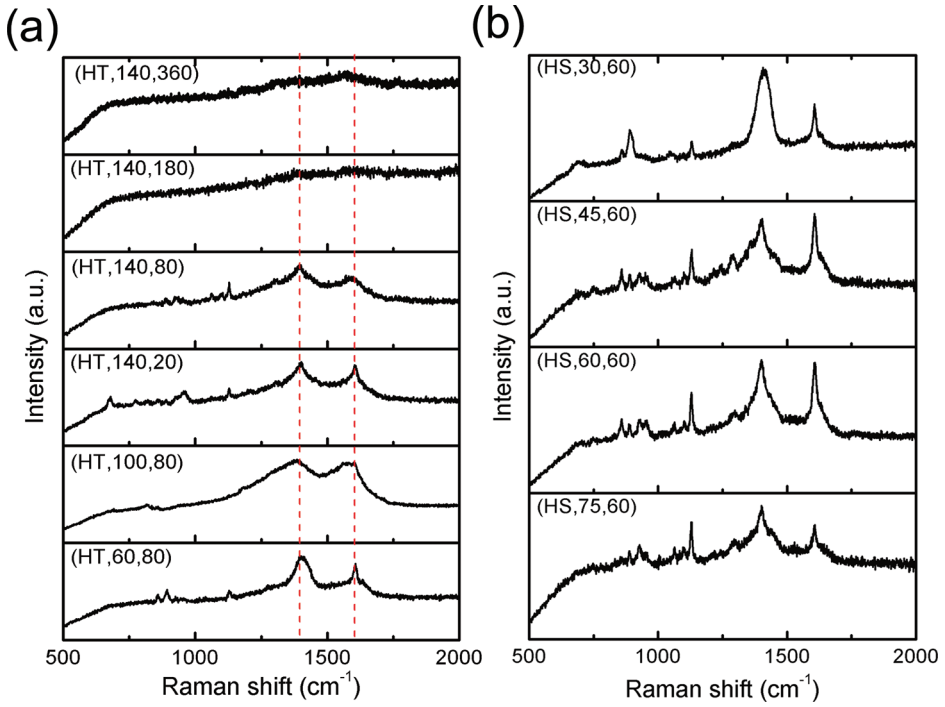


Figure 2. Solution-phase Raman spectra of as-prepared AgNPs by (a) the HT method and (b) the HS method.

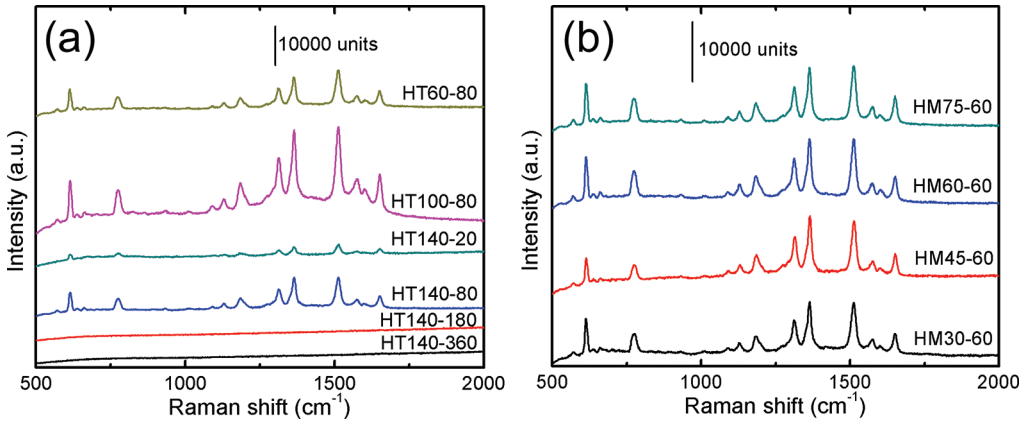


Figure 3. SERS spectra of R6G (10^{-6} M) mixed with colloidal AgNPs prepared by (a) the HT method and (b) the HS method under different reaction conditions.

lengths using PVP as the surfactant, and they have measured the Raman spectra of as-prepared samples.[21] The Raman signal from PVP has been detected, indicating that PVP remains on the surface of the Ag nanocubes. In our experiment, PVP was also used as the stabilizer; however, apart from the two broad peaks, no Raman signal from PVP was observed. To eliminate the possibility of two broad carbon-related peaks produced due to the fact that the laser power used in the experiment is too high to induce the decomposition of part of PVP on the surfaces of AgNPs, Raman spectra of the pure PVP were measured under the same conditions (not show here), where no carbon-related peaks but only Raman signals originated from PVP are observed. The other eliminating method is to compare the Raman spectra of colloidal AgNPs prepared under different conditions. Supposing that carbon on the AgNPs is formed by the laser induced damage of PVP, then the carbon signal among colloidal AgNPs prepared under different conditions should be similar or basically the same. However, Figure 2a shows that, when the heating time is longer than 180 min, the intensities of two carbon peaks become very weak, which contradicts the above hypothesis. This indicates that carbon on the AgNPs is not originated from PVP, and it is very possible that carbon films with different thicknesses formed on the AgNP surfaces (corresponding to the changes of carbon signal intensity), which has been fully confirmed in the later sections. As shown in Figure 2b, in addition to some small peaks, two broad carbon peaks are also observed, similar to those for AgNPs prepared by the HT method. In addition, no large differences have been found among the AgNPs prepared by the HS method at different temperatures.

3.2. Comparison of SERS Properties of As-Prepared AgNPs under Different Conditions. Figure 3 compares the SERS signal intensities of R6G (10^{-6} M) obtained from colloidal AgNPs prepared under different reaction conditions. As shown in Figure 3a, the intensities of SERS signals from colloidal AgNPs with the same concentration are strongly

dx.doi.org/10.1021/jp3018088 | J. Phys. Chem. C 2012, 116, 12283−12294

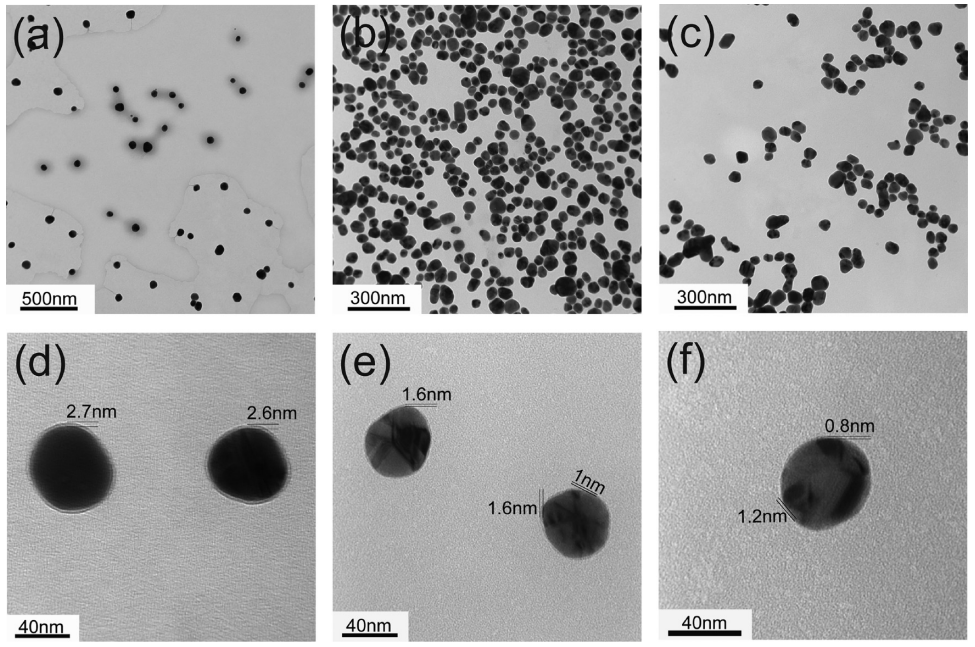


Figure 4. TEM images of (a) AgNP(HT,140,360), (b) AgNP(HT,100,80), and (c) AgNP(HS,60,60). (d–f) The corresponding HRTEM images of AgNPs in parts a–c.

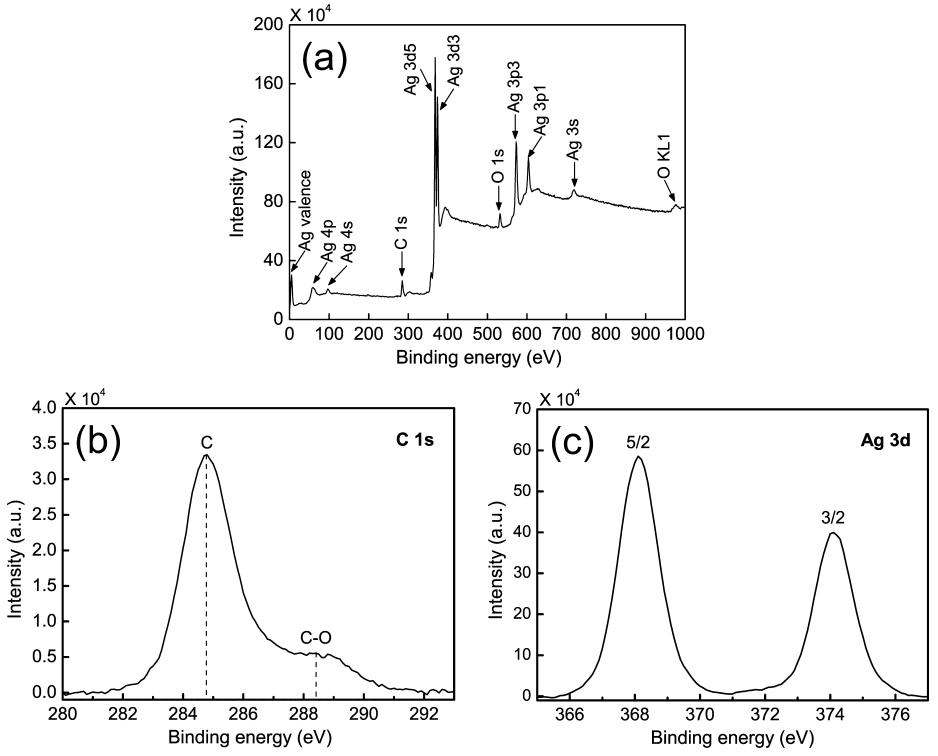


Figure 5. (a) Survey XPS spectrum of AgNP(HT,140,360), (b) C1s, and (c) Ag3d fine XPS spectra of AgNP(HT,140,360).

dependent on the reaction time and temperature. It is clearly observed that the SERS signal from AgNP(HT,140,80) is stronger than that of AgNP(HT,140,20). The SERS difference between AgNP(HT,140,80) and AgNP(HT,140,20) is considered to be due to the size effect. However, with colloidal AgNPs prepared at 140 °C for longer than 180 min, no SERS or very extremely weak signals were detected. Compared with the SERS signals for AgNPs prepared at different temperatures, the intensity of SERS signal from the AgNP(HT,100,80) is about 4.8 and 2.3 times stronger than those of AgNP(HT,140,80) and AgNP(HT,60,80), respectively. Figure 3b shows a comparison of SERS spectra from AgNPs prepared by the HS method at four different heating temperatures of 30, 45, 60, and 75 °C (from bottom to top in the plot). There seems to be no large differences in intensity of SERS signals with increasing heating temperature (the SERS signal corresponding to AgNP(HM,30,60) seems a little lower), which indicates that

dx.doi.org/10.1021/jp3018088 | J. Phys. Chem. C 2012, 116, 12283–12294

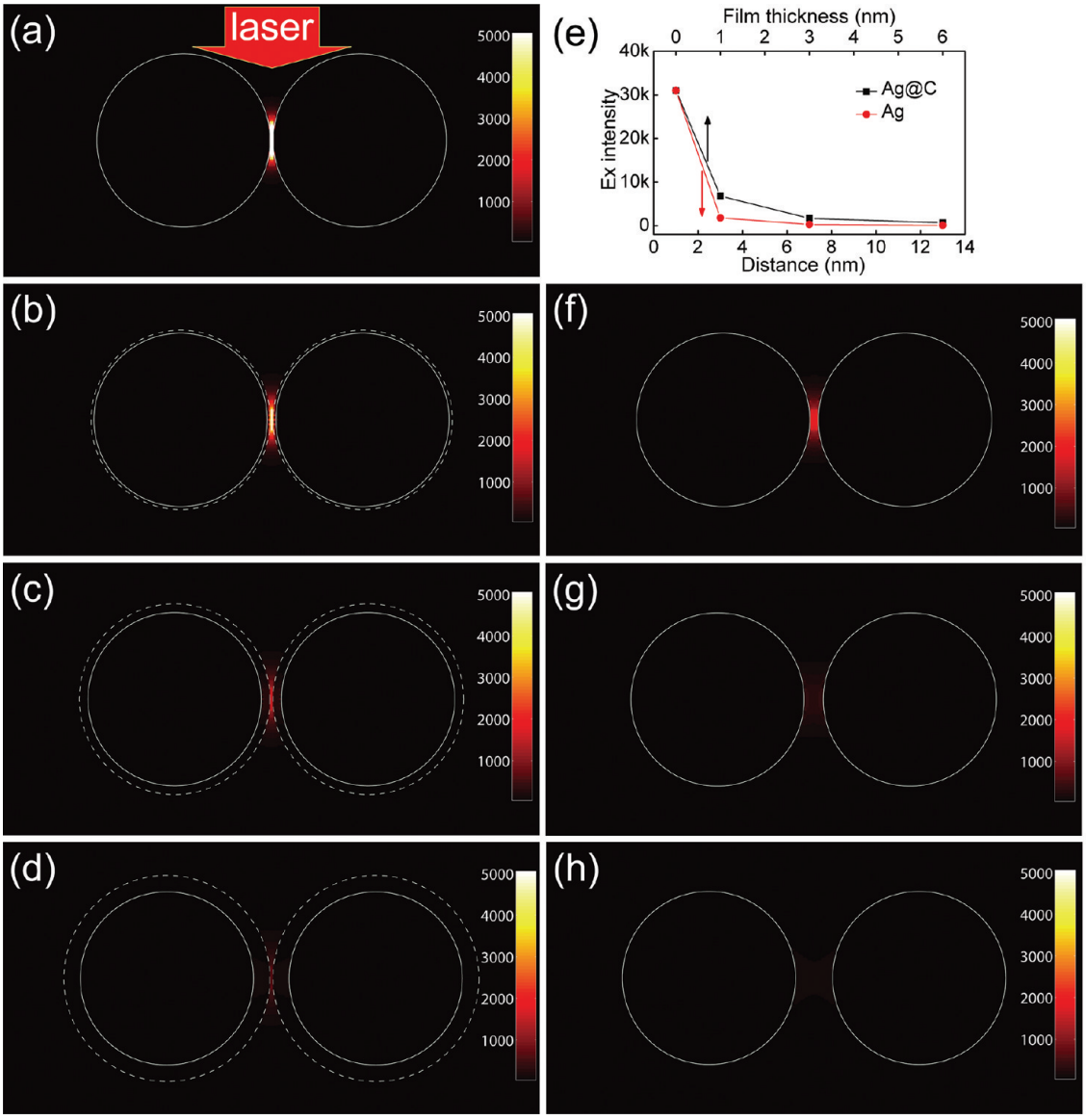


Figure 6. FDTD simulation of E-field distributions at the gap between two adjacent (a) Ag, (b) Ag@1 nmC, (c) Ag@3 nmC, and (d) Ag@6 nmC NPs. The radius of AgNP is 30 nm. The shell to shell distance is 1 nm. (e) The film thickness or distance dependence of E-field intensity in the center of two Ag@C NPs or AgNPs. FDTD simulation of E-field distributions between two adjacent bare Ag spheres with distances ranging from (f) 3 nm to (g) 7 nm to (h) 13 nm. Laser wavelength: 632.8 nm.

AgNPs prepared by the HS method at temperatures ranging from 30 to 75 °C have similar SERS activity.

At the same time, a question is raised of why AgNPs prepared by the HT method under different temperatures and times exhibit such large differences in SERS activity. Raman spectra indicate that AgNP(HT,100,80) have the highest SERS activity, while AgNP(HT,140,180) and AgNP(HT,140,360) exhibit very low SERS activities. It is known that SERS strongly depends on the detailed physical structure of a metal nanomaterial, including its size, shape, morphology, and composition.[21−23] According to the above UV−visible absorption and AFM analysis, heating temperature and reaction time only affect the sizes of the grown AgNPs. However, there is no significant difference among the sizes of these AgNPs. Therefore, the particle size difference is not considered to be the main factor that affects the SERS difference.

To investigate the main causes of the SERS difference, TEM images of different colloidal AgNPs have been compared. Parts a and b of Figure 4 show the TEM images of AgNPs prepared by the HT method at 140 °C for 360 min (no SERS activity) and at 100 °C for 80 min (high SERS activity), respectively. It is found that the sizes of these NPs are slightly different, corresponding to the UV−visible absorption and AFM observation. A careful observation in Figure 4a shows that most of the AgNPs are covered by a thick membrane, which is not discovered in Figure 4b. This membrane may be originated from glucose or its derivative. Figure 4c shows the TEM image of AgNPs prepared by the HS method at 60 °C for 60 min (SERS active) and no membrane has been observed, similar to Figure 4b. Parts d−f of Figure 4 show the corresponding HRTEM images of AgNPs shown in parts a−c. As shown in Figure 4d, each AgNP is covered by a uniform thick film with a thickness of approximately 2.7 nm, forming a core−shell structure. Similarly, AgNPs shown in Figure 4e and f are also surrounded by a film, but the films are much thinner and not very uniform, approximately 1−1.6 and 0.8−1.2 nm,

dx.doi.org/10.1021/jp3018088 | J. Phys. Chem. C 2012, 116, 12283−12294

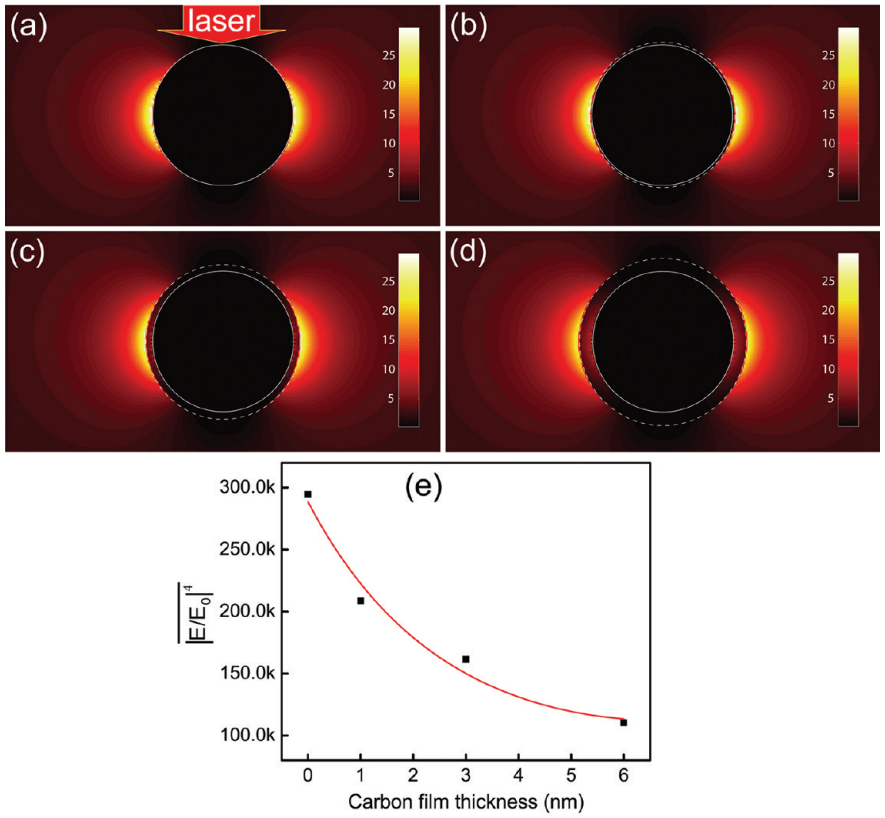


Figure 7. Comparison of E-field enhancement for a single AgNP with different carbon-shell thicknesses: (a) Ag, (b) Ag@1 nmC, (c) Ag@3 nmC, and (d) Ag@6 nmC NPs. The radius of AgNP is 30 nm. Laser wavelength: 632.8 nm. (e) Dependence of the average SERS EF $\overline{|E/E_0|^4}$ on the carbon film thickness.

respectively. In order to identify the composition of the film, XPS analysis was made. Figure 5a shows the survey XPS spectra for the as-prepared AgNPs by the HT method at 140 °C for 360 min. It can be observed that AgNPs are at a high purity, with only a small amount of carbon and very little oxygen. The C(1s) XPS spectrum of AgNP(HT,140,360) is shown in Figure 5b. In addition to the C(1s) peak at 284.8 eV, the C−O peak at 288.5 eV is also observed. This is a clear indication that the films coated on the surfaces of AgNPs are composed of carbon. Namely, Ag@C core−shell NPs can be obtained by using the present HT and HS methods. Similarly, Fang et al. have synthesized Ag@C nanostructures (core−shell NPs and nanocables) through reduction of Ag^+ with ascorbic acid in the presence of CTAB under hydrothermal conditions.[11] Two evolution stages were considered in the formation process: (1) synthesis of AgNPs in the restriction of CTAB, (2) carbonization of ascorbic acid and then formation of an amorphous carbon layer on the AgNP surface. Figure 5c shows the Ag3d fine XPS spectrum of Ag NP (HT,140,360) with carbon film thickness of approximately 2.7 nm. The binding energy of $Ag3d_{5/2}$ is at 368.1 eV and the binding energy of $Ag3d_{3/2}$ is at 374.1 eV, which indicates that only Ag(0) binding exists in the AgNPs. The above XPS analysis suggests that a carbon layer with a thickness larger than 2.7 nm is thick enough to protect the AgNPs against oxidation. It is also observed in Figure 4 that the thickness of the carbon shell is gradually increased by rising the reaction temperature and time. The above experimental results indicate that Ag@C NPs with a thick carbon film have a very low SERS activity; on the contrary, strong SERS signals can be observed for the AgNPs with ultrathin film. Therefore, carbon shell thickness is considered to be the key factor that affects SERS difference. In addition, the SERS activities of two kinds of AgNPs with and without carbon shells have been compared, as shown in Figure S5 in the Supporting Information. The detailed results have been explained in section 2.3 of the Supporting Information.

It is known that SERS can be attributed to two mechanisms, the electromagnetic enhancement due to the localized surface plasmon resonance (LSPR) mode and chemical enhancement that arises from the interaction between molecules and NPs. In this report, R6G is selected because of its good absorbability on silver surfaces.[24] In addition, the amorphous carbon film on the AgNP surface is hydrophilic, which is chemically compatible with R6G solution, so that R6G molecules are also easily absorbed onto Ag@C NP surfaces.[17] Therefore, the difference in the affinity or the number of probed R6G molecules between Ag@C and bare silver NPs in the Raman measurements can be ruled out. Then, the electromagnetic mechanism is considered to contribute most of the enhancement. In this experiment, the weak electric field (E-field) is produced between the adjacent AgNPs with a thick carbon film; on the contrary, the strong E-field is produced between the adjacent AgNPs with an ultrathin film. In order to further understand the influence of carbon shell thickness on the field enhancement, a theoretical simulation was carried out by using the FDTD method. Figure 6 illustrates the calculated optical E-field distribution between two adjacent Ag@C NPs or AgNPs. As shown in Figure 6a, localized surface plasmon can be excited in the nanocaps between two Ag spheres (so-called hot spots), producing a strong E-field enhancement and subsequently a great increase

dx.doi.org/10.1021/jp3018088 | J. Phys. Chem. C 2012, 116, 12283−12294

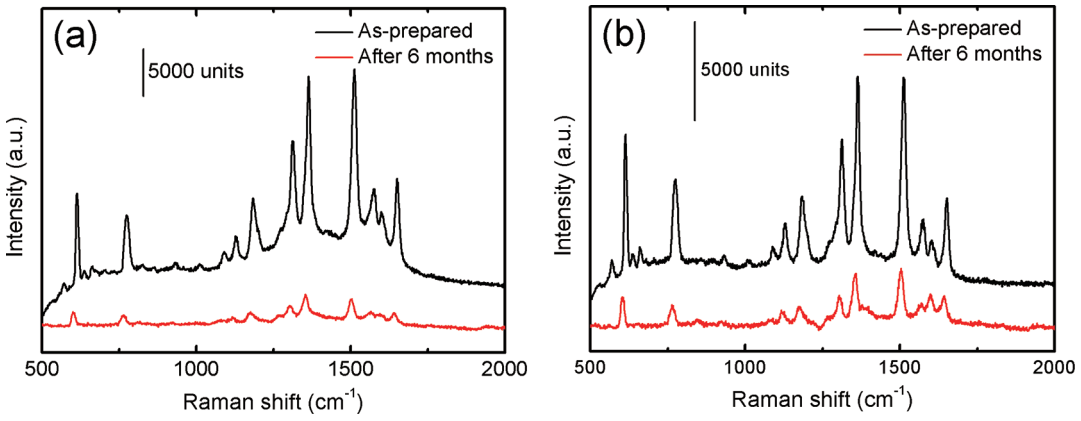


Figure 8. The effect of shelf life on the SERS enhancement: (a) R6G(10^{-6} M)/AgNP(HT,100,80); (b) R6G(10^{-6} M)/AgNP(HS,60,60).

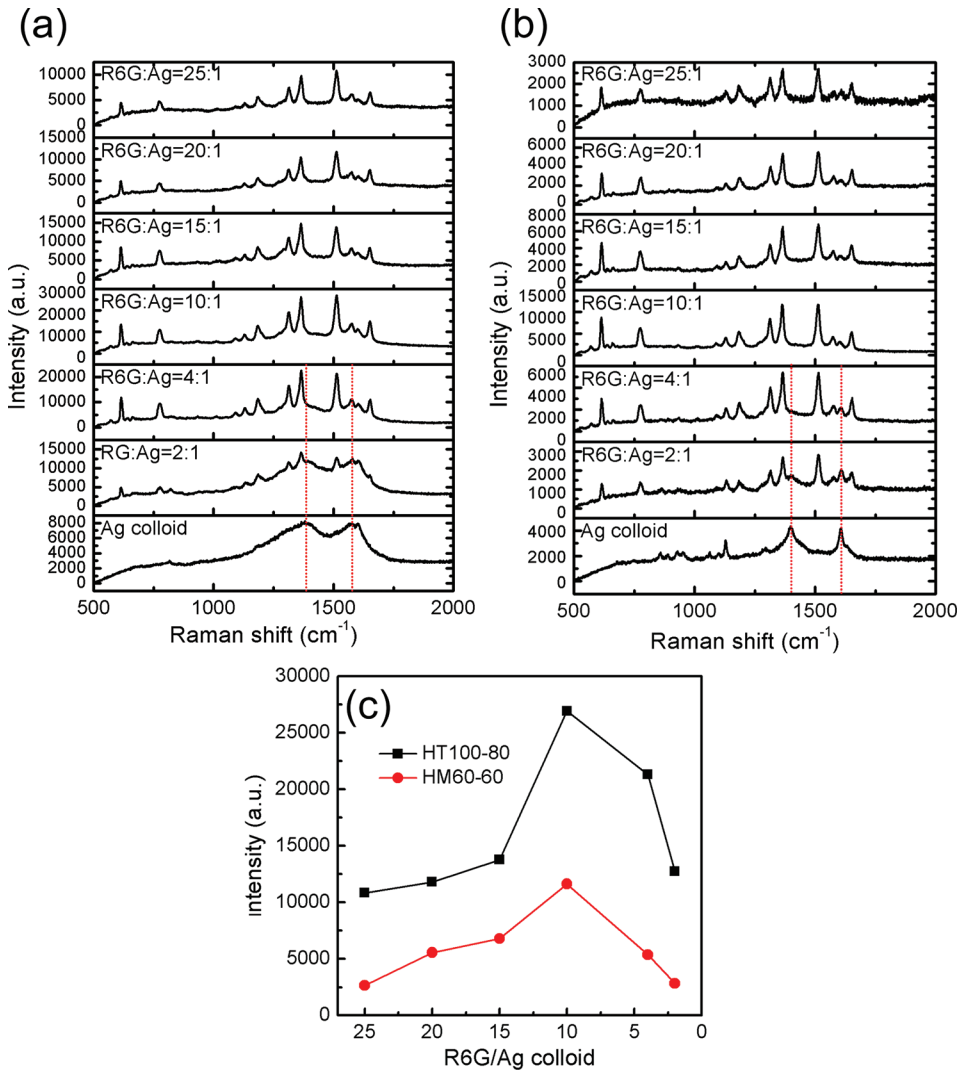


Figure 9. The dependence of SERS intensity on the R6G/AgNP volume ratio: (a) R6G(10^{-6} M)/AgNP(HT,100,80); (b) R6G(10^{-6} M)/AgNP(HS,60,60). (c) The variation of the 1512 cm^{-1} band (C−C) intensity with R6G/AgNP volume ratio.

of the Raman intensity for molecules on the sphere surface. Parts b−d of Figure 6 show the E-field distributions between two AgNPs with carbon-shell thicknesses of 1, 3, and 6 nm, respectively. It can be clearly seen that the E-field enhancement for the thin carbon shell is stronger than that for the thick carbon shell. To more quantitatively investigate the relation between the shell thickness and the E-field intensity, the dependence of E-field intensity on carbon-shell thickness is plotted in Figure 6e (black points). It can be observed in Figure 6e that the signal decreases exponentially with increasing thickness. In fact, increasing the carbon-shell thickness corresponds to increasing the spacing of AgNPs. Because the

dx.doi.org/10.1021/jp3018088 | J. Phys. Chem. C 2012, 116, 12283−12294

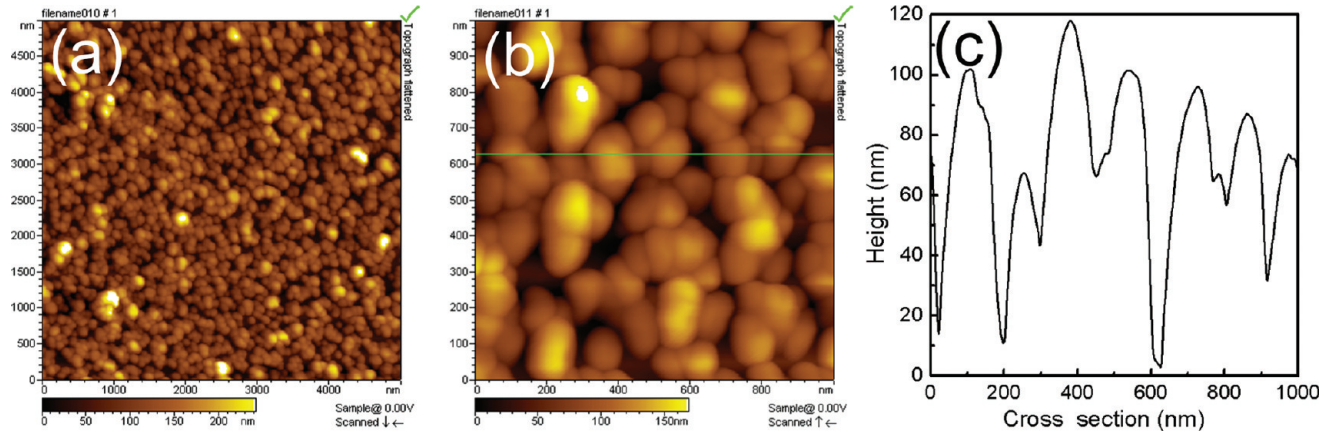


Figure 10. (a) Low and (b) high magnification AFM images of AgNP(HS,60,60) film prepared by a spin-coating method. (c) The cross section of the line in part b.

E-field intensity and SPR enhancement of Raman scattering largely depend on the spacing of NPs or nanostructures, a weak E-field is produced by AgNPs with a thick carbon shell. Figure 6f–h show the E-field distributions between two adjacent bare Ag spheres with interparticle distances of 3, 7, and 13 nm, respectively. Compared with the E-field distributions produced between two Ag@C NPs and two bare AgNPs with the same inter-AgNP distances (3 nm in Figure 6b and f, 7 nm in Figure 6c and g, 13 nm in Figure 6d and h), the E-field intensities produced in the gap between Ag@C NPs are stronger than those between bare AgNPs (3.78, 5.67, and 7.37 times stronger for 3, 7, and 13 nm, respectively). However, this could not prove whether the carbon layer can lead to the SERS enhancement. To confirm this, the E-field and the average SERS enhancement for a single AgNP with different carbon layer thickness have been calculated, as shown in Figure 7. It can be observed that there is no large difference in field enhancement between bare AgNP (Figure 7a) and Ag@C NP (Figure 7b–d). The average SERS enhancement factor (EF) over the entire surface of each NP has also been compared, where SERS EF is simply defined as $(E/E_0)^4$ (E_0 is the incident field). It is shown in Figure 7e that the average SERS EF is gradually decreased with the increase of the carbon layer thickness, indicating that the carbon layer has no positive action to SERS enhancement. On the basis of experimental results and simulation analysis, a conclusion can be made that AgNPs with an ultrathin carbon shell are desired to obtain a strong SERS enhancement. The carbon layer has two main functions of protecting the AgNPs against oxidation and controlling the spacing of AgNPs.

3.3. Effects of Shelf Life and Colloidal AgNP Concentration on SERS Enhancement. Stability of the noble metal NPs is always a significant issue. For the colloids, there is a large problem because of the potential of the particles to aggregate and to chemically react with other compounds present in the aqueous solution. Therefore, Ag colloids usually exhibit a relatively short shelf life (i.e., days). To characterize the shelf life of AgNPs prepared by HT and HS methods, the as-prepared AgNPs were stored at 4 °C in an incubator for a period of time before measurement. Figure 8 shows the SERS spectra of R6G (10^{-6} M) mixed with colloidal AgNPs stored for 0 and 6 months. It can be seen that, for AgNP(HT,100,80), the SERS signals are decreased by approximately 6 times for a long period of 6 months (Figure 8a), while the SERS enhancement from AgNP(HS,60,60) is decreased by approximately 3.5 times (Figure 8b). The shell-life of AgNP-(HS,60,60) is similar to that of AgNP(HT,100,80), because they have the similar carbon shell thickness. It is considered that carbon defects may exist in the ultrathin carbon shells of Ag@C NPs, which lead to the decrease of Ag@C NP SERS activity. Overall, the slow decrease in SERS enhancement after such a long time of storage demonstrates that AgNPs prepared by the HT and HS methods have a long shelf life, which is mainly due to the formed carbon shell on the AgNP surfaces. This kind of Ag@C core–shell nanostruture may provide them with the potential for uses as SERS-active and as stable NPs in many applications.

For a given concentration of R6G, the intensity of SERS signal also depends on the volume ratio of R6G to colloidal AgNPs, that is, on the formal concentration or the total number of the silver particles in the R6G solution. Figure 9 shows two examples of SERS intensity dependence on the R6G/AgNP volume ratio, (a) R6G(10^{-6} M)/AgNP(HT,100,80) and (b) R6G(10^{-6} M)/AgNP(HS,60,60). In Figure 9a, the Raman signal intensity increases gradually with decreasing R6G/AgNP volume ratio (from top to bottom), and the intensity reaches a maximum when their volume ratio is 10:1. However, a further decrease in the volume ratio results in a strong decrease of signal intensity. Meanwhile, two broad Raman peaks originated from colloidal AgNPs have been emerged in the spectra, as indicated by two red dashed lines. A similar phenomenon is also observed in Figure 9b, that the signal increases to a maximum and then decreases with decreasing R6G(10^{-6} M)/AgNP(HS,60,60) volume ratio. Figure 9c shows the variation of band (C–C) intensity at (or near) 1512 cm^{-1} with R6G/AgNP volume ratio, from which a clear relationship between SERS intensity and R6G/AgNP volume ratio can be observed. The interplay between concentration of colloidal AgNPs and SERS signal intensity is rather complex due to several factors that determine the SERS enhancement. Provided that the same concentration of R6G is present in the solution, then the SERS enhancement mainly depends on the interspacing of adjacent AgNPs (i.e., the concentration of colloidal AgNPs) and on the number of R6G molecules that can be adsorbed on the particle surfaces. Then, the SERS signal rises with increasing concentration of AgNPs as long as this concentration increase results in an increase in the total number of R6G molecules on the particle surfaces. If the concentration of AgNPs is increased too much, then the average number of R6G on each particle surface is reduced, and therefore the SERS signal of R6G is

dx.doi.org/10.1021/jp3018088 | J. Phys. Chem. C 2012, 116, 12283–12294

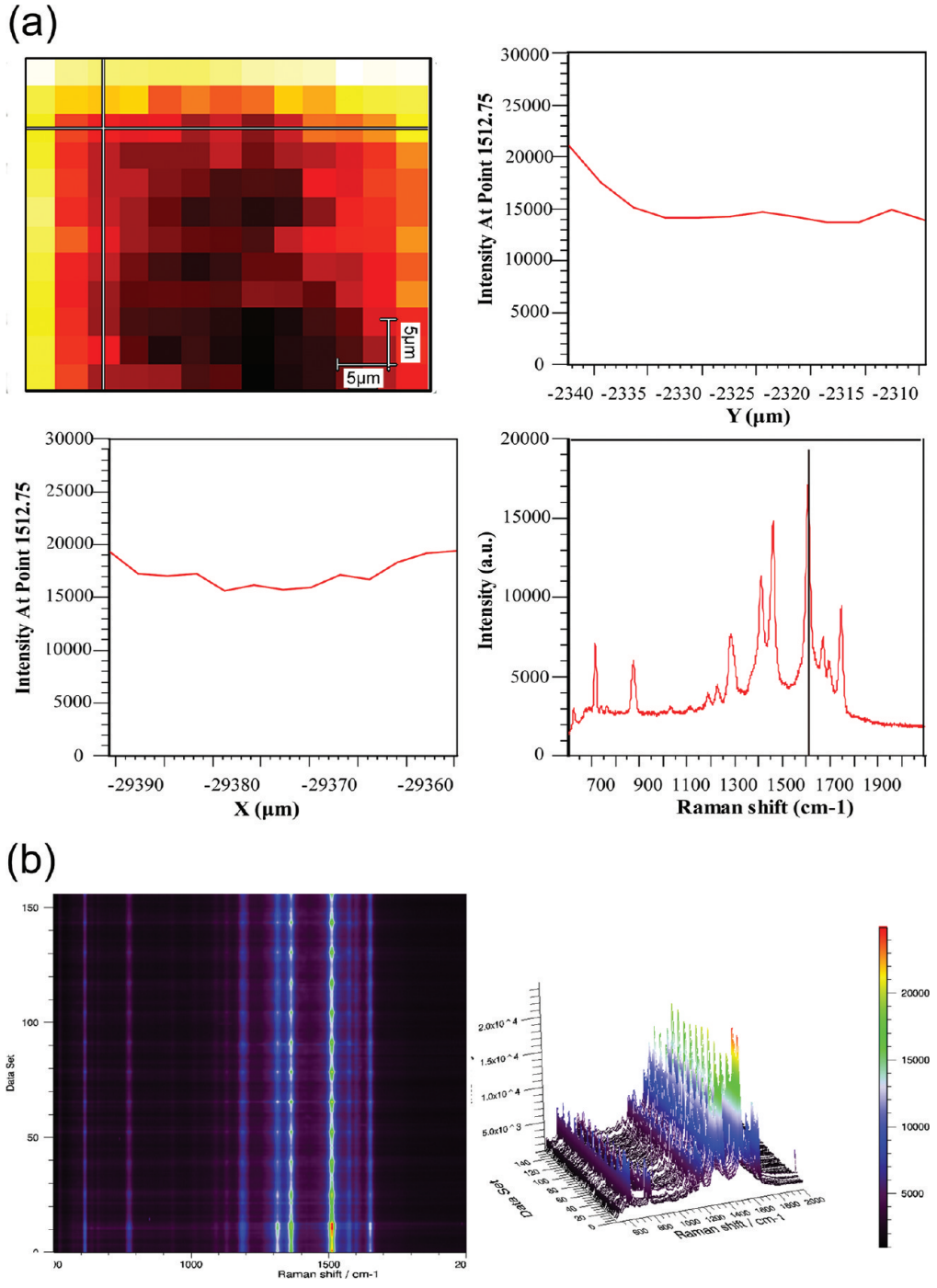


Figure 11. SERS mapping (step size, 3 μm; mapping area, 13 × 12 = 157 points) of R6G with a concentration of 10^{-7} M on AgNP(HS,60,60) film. (a) The mapping view (the top left illustrates the measured rectangular region and the brightness is proportional to the R6G signal intensity at 1512.75 cm^{-1}, the top right and bottom left are the corresponding sectional views of the two crossed lines, the bottom right is the spectral line of the intersection and the vertical black lines show the location of the selected Raman shift of 1512.75 cm^{-1}). (b) The bird's-eye view and surface view of the Raman mapping.

decreased and the Raman signal from colloidal AgNPs appears. Therefore, in order to obtain a high SERS intensity, the volume ratio of probe molecules and colloidal AgNPs should be optimized.

3.4. SERS Substrate Preparation. So far, various SERS substrates have been fabricated by using electron beam lithography, nanoimprint lithography, templated assembly of NPs, and NP-coated silicon nanowire arrays, etc.[25−29] In these methods, templated self-assembly is employed utilizing the chemical interaction between NPs and the surface of substrate, which may introduce additional information during the SERS measurement. For the lithograph, though it can produce an ordered pattern and can control the density of NP distribution; however, this method is complicated and expensive, not suitable for mass production of SERS substrate.

Therefore, a simple spin-coating method has been proposed, which has been widely applied in many aspects.[30−32] In this report, 10 μL of AgNP(HS,60,60) alcoholic solution was spin-

dx.doi.org/10.1021/jp3018088 | J. Phys. Chem. C 2012, 116, 12283−12294

coated on a Si substrate (size: 8 × 8 mm^2) with a rotating speed of 1200 rpm and then a AgNP(HS,60,60) thin film was obtained, which can be used as the active SERS substrate. Figure 10 shows the AFM topographic images and the corresponding cross section of AgNP(HS,60,60) film prepared by the spin-coating method. It is observed that one to two layers of AgNPs with a height of approximately 120 nm are formed. In addition, AgNPs distribute densely and uniformly on the whole substrate, which is consistent with the SEM images shown in Figure S7 in the Supporting Information. This kind of nanostructure may exhibit enormous E-field enhancement in the gaps between adjacent NPs, creating uniform densities of "hot spots" for the large SERS enhancement.

Figure 11 shows the Raman mapping (step size: 3 μm, mapping area: 13 × 12 = 157 points) of R6G with a concentration of 10^{-7} M on the AgNP(HS,60,60) film. As shown in Figure 11a, the top left illustrates the measured rectangular region and the brightness is proportional to the R6G signal intensity at 1512.75 cm^{-1}; the top right and bottom left are the corresponding sectional views of the two crossed lines; the bottom right is the spectral line of the intersection, and the vertical black line shows the location of the selected Raman shift of 1512.75 cm^{-1}. Figure 11b shows the bird's-eye view (left) and surface view (right) of the Raman mapping. A strong signal intensity of R6G with low concentration can be detected, indicating that this substrate has a high SERS enhancement. It is noted that Figure 11b and the top left image in Figure 11a show a uniform spectra intensity, which reveals that the AgNP film prepared by the spin-coating method can be used as a uniform and reproducible SERS substrate.

4. CONCLUSIONS

We have described a facile and versatile method for the growth of AgNPs under hydrothermal and low temperature heating–stirring conditions using glucose as the reducing agent. The morphology and SERS activity of the AgNPs prepared under different conditions have been compared. It is found that reaction conditions affect greatly the sizes and distributions of AgNPs. The as-prepared AgNPs under different conditions exhibit a large difference in SERS activity, which is mainly due to the fact that carbon shells with different thicknesses are formed on the NP surface. This kind of Ag@C NPs with an ultrathin film exhibits high SERS activity and long shelf life. The carbon layer has two main functions of protecting the AgNPs against oxidation and controlling the spacing of AgNPs. In addition, the AgNP film SERS substrate has been prepared by a simple spin-coating method, which exhibits high SERS activity, uniformity, and reproducibility.

■ ASSOCIATED CONTENT

Supporting Information

AFM images of AgNPs prepared by HT and HS methods; growth of AgNPs by the microwave heating (MH) method; SEM images of AgNP film prepared by a spin-coating method. This material is available free of charge via the Internet at http://pubs.acs.org.

■ AUTHOR INFORMATION

Corresponding Author

*Phone: +86-411-84707863-334. Fax: +86-411-84709304. E-mail: lpan@dlut.edu.cn.

Notes

The authors declare no competing financial interest.

■ ACKNOWLEDGMENTS

This work was supported by the National Natural Science Foundation of China (No. 11074029 and No. 61137005) and the Fundamental Research Funds for the Central Universities (No. DUT12ZD204).

■ REFERENCES

(1) Balan, L.; Malval, J. P.; Schneider, R.; Burget, D. *Mater. Chem. Phys.* **2007**, *104* (2–3), 417–421.
(2) Park, S. J.; Kim, S.; Lee, S.; Khim, Z. G.; Char, K.; Hyeon, T. *J. Am. Chem. Soc.* **2000**, *122* (35), 8581–8582.
(3) Jana, N. R.; Pal, T. *Langmuir* **1999**, *15* (10), 3458–3463.
(4) Jeanmaire, D. L.; Vanduyne, R. P. *J. Electroanal. Chem.* **1977**, *84* (1), 1–20.
(5) Kneipp, J.; Kneipp, H.; Kneipp, K. *Chem. Soc. Rev.* **2008**, *37* (5), 1052–1060.
(6) Qian, X. M.; Nie, S. M. *Chem. Soc. Rev.* **2008**, *37* (5), 912–920.
(7) Singh, P.; Thuy, N. T. B.; Aoki, Y.; Mott, D.; Maenosono, S. *J. Appl. Phys.* **2011**, *109* (9), 094301(7).
(8) Xiong, Y. J.; Washio, I.; Chen, J. Y.; Cai, H. G.; Li, Z. Y.; Xia, Y. N. *Langmuir* **2006**, *22* (20), 8563–8570.
(9) Lee, K. H.; Rah, S. C.; Kim, S. G. *J. Sol-Gel Sci. Technol.* **2008**, *45* (2), 187–193.
(10) Kim, H. S.; Lee, K. H.; Kim, S. G. *Aerosol Sci. Technol.* **2006**, *40* (7), 536–544.
(11) Fang, Z.; Tang, K. B.; Lei, S. J.; Li, T. W. *Nanotechnology* **2006**, *17* (12), 3008–3011.
(12) Wang, Z. H.; Liu, J. W.; Chen, X. Y.; Wan, J. X.; Qian, Y. T. *Chem.—Eur. J.* **2004**, *11* (1), 160–163.
(13) Liu, B. L. *Mater. Rev.* **2010**, *24* (3), 132–134.
(14) Mori, Y.; Tagawa, T.; Fujita, M.; Kuno, T.; Suzuki, S.; Matsui, T.; Ishihara, M. *J. Nanopart. Res.* **2011**, *13* (7), 2799–2806.
(15) Wei, S. Y.; Wang, Q.; Zhu, J. H.; Sun, L. Y.; Lin, H. F.; Guo., Z. H. *Nanoscale* **2011**, *11* (3), 4474–4502.
(16) Li, J. F.; Huang, Y. F.; Ding, Y.; Yang, Z. L.; Li, S. B.; Zhou, X. S.; Fan, F. R.; Zhang, W.; Zhou, Z. Y.; Wu, D. Y.; Ren, B.; Wang, Z. L.; Tian, Z. Q. *Nature* **2010**, *464* (7287), 392–395.
(17) Liu, F. S.; Cao, Z. S.; Tang, C. J.; Chen, L.; Wang, Z. L. *ACS Nano* **2010**, *4* (5), 2643–2648.
(18) Liu, F. S.; Tang, C. J.; Pan, J.; Cao, Z. S.; Wang, Z. L. *J. Phys. Chem. C* **2010**, *114* (21), 9871–9875.
(19) Liu, F. S.; Yao, K. L.; Liu, Z. L. *Diamond Relat. Mater.* **2007**, *16* (9), 1746–1751.
(20) Liu, F. X.; Wang, Z. L. *Surf. Coat. Technol.* **2009**, *203* (13), 1829–1832.
(21) Zhang, Q. A.; Li, W. Y.; Moran, C.; Zeng, J.; Chen, J. Y.; Wen, L. P.; Xia, Y. N. *J. Am. Chem. Soc.* **2010**, *132* (32), 11372–11378.
(22) Rycenga, M.; Cobley, C. M.; Zeng, J.; Li, W. Y.; Moran, C. H.; Zhang, Q.; Qin, D.; Xia, Y. N. *Chem. Rev.* **2011**, *111* (6), 3669–3712.
(23) Maxwell, D. J.; Sr, E.; Nie, S. M. *Chem. Mater.* **2001**, *13* (3), 1082–1088.
(24) Kneipp, K.; Wang, Y.; Dasari, R. R.; Feld, M. S. *Appl. Spectrosc.* **1995**, *49* (6), 780–784.
(25) Stiles, P. L.; Dieringer, J. A.; Shah, N. C.; Van Duyne, R. R. *Annu. Rev. Anal. Chem.* **2008**, *1*, 601–626.
(26) Lee, S. J.; Guan, Z. Q.; Xu, H. X.; Moskovits, M. *J. Phys. Chem. C* **2007**, *111* (49), 17985–17988.
(27) Hering, K.; Cialla, D.; Ackermann, K.; Dorfer, T.; Moller, R.; Schneidewind, H.; Mattheis, R.; Fritzsche, W.; Rosch, P.; Popp, J. *Anal. Bioanal. Chem.* **2008**, *390* (1), 113–124.
(28) Wu, Y. K.; Liu, K.; Li, X. F.; Pan, S. *Nanotechnology* **2011**, *22* (21), 215701(6).
(29) Wang, H.; Levin, C. S.; Halas, N. J. *J. Am. Chem. Soc.* **2005**, *127* (43), 14992–14993.

(30) Haubner, R.; Schwinger, W.; Haring, J.; Schoftner, R. *Diamond Relat. Mater.* **2008**, *17* (7−10), 1452−1457.
(31) Li, D. W.; Pan, L. J. *J. Mater. Res.* **2011**, *26* (16), 2024−2032.
(32) Chou, K.-S.; Huang, K.-C.; Lee, H.-H. *Nanotechnology* **2005**, *16* (6), 779−784.